THE JOURNAL OF PHYSICAL CHEMISTRY A

Article

pubs.acs.org/JPCA

Anion Photoelectron Spectroscopy and CASSCF/CASPT2/RASSI Study of La_n^- (n = 1, 3−7)

A. S. Ivanov,[†,#] X. Zhang,[‡,#] H. Wang,[‡] A. I. Boldyrev,[†,§] G. Gantefoer,[‡] K. H. Bowen,[‡] and I. Černušák*[,§]

[†]Department of Chemistry and Biochemistry, Utah State University, 0300 Old Main Hill, Logan, Utah 84322-0300, United States

[‡]Department of Chemistry, Johns Hopkins University, Baltimore, Maryland 21218, United States

[§]Department of Physical and Theoretical Chemistry, Faculty of Natural Sciences, Comenius University in Bratislava, Mlynská dolina CH1, 84215 Bratislava, Slovakia

Supporting Information

ABSTRACT: We present a combined experimental and theoretical study of small lanthanum clusters. The experimental photoelectron spectra of La_n^- (n = 1, 3−7) were obtained using negative ion photoelectron spectroscopy. Electron affinities for these clusters were found to be in a range of 0.49 eV (La) to 1.5 eV (La_7). Our computational *tour de force* in exploring the electronic structure and its consequences for the lanthanum atom and its anion as well as for lanthanum trimer and its anion shows the multiconfigurational method and large basis set with spin−orbit corrections: CASSCF/CASPT2/RASSI/ANO-RCC-L level of theory is needed to reproduce experimental accuracy. The most stable structure for La_3^- was established to be an equilateral triangle ($^1A_1'$). Chemical bonding analysis of the La_3^- global minimum reveals that this is the first experimentally observed species with d-AO double σ and π aromaticity.

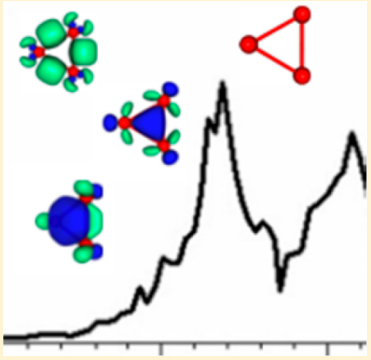

I. INTRODUCTION

Lanthanum sits at the beginning of the lanthanide series, having the electronic configuration [Xe]5d6s^2; it is the only rare earth element which does not fill the 4f shell. This metal has applications in optical fibers, nonlinear optical crystals,[1] ZBLAN fluoride glasses,[2] catalysts,[3] electron cathodes,[4,5] scintillators,[6] doping materials for the fuel cells, and in studio lighting and projection. In order to enable the utilization of this metal at the subnanoscale, studies of the molecular clusters of La are desirable. Among the molecular properties pertinent to gas-phase clusters, the electron affinity (EA) is an important property extensively used in describing electron donor/acceptor behavior and charge-transfer processes. The EA of the La atom has been measured by anion photoelectron spectroscopy to be 0.47 ± 0.02 eV.[7] However, it appears that no electron affinity values have been measured for larger lanthanum clusters. From the computational point of view, the electron affinities of lanthanum clusters represent a challenging task. Due to their complicated valence electronic structure and bonding, one can expect both multiconfiguration natures and significant relativistic effects. Several gas-phase studies on the structure and energetics of small neutral La clusters embedded in different chemical environments have been published recently.[8−14] An earlier experimental attempt by Knight and co-workers[15] failed to observe the isolated La_3 molecule and led to the conclusion that it either does not exist or acquires linear form. It is noteworthy that their results indicate the corresponding lighter transition-metal cluster Sc_3 is triangular, while Y_3 is either linear or bent.

Negative ions can be fragile species with relatively weak binding energies (EA) between the excess electron and its neutral atom/molecule. Typically, electron affinities range from a few tenths to several electron volts. EA is a crucial quantity for better understanding of the properties of negative ions and their interaction with the environment. Negative ions are important in astrophysics, atmospheric chemistry/physics (in particular, in the D region of the Earth's ionosphere[16]), gas-phase chemical reactivity, plasma physics, and materials processing (plasma etching industry). The development of negative ion sources is crucial for neutral beam heating systems in Tokamaks.[17] The importance of negative ions is also reflected by a series of reviews collecting our knowledge of these extraordinary species.[18−20]

The most valuable experimental technique for determining EA values is gas phase anion photoelectron spectroscopy (aPES).[21,22] Here, we present the results of a joint aPES/computational investigation of La clusters and their anions. On the basis of quantum-chemical calculations, we also present the interpretation of the anion photoelectron spectra of the La/La^- and La_3/La_3^- species.

II. EXPERIMENTAL METHODS

Negative ion photoelectron spectroscopy is conducted by crossing a mass-selected beam of anions with a fixed frequency

Received: August 19, 2015
Revised: October 23, 2015

DOI: 10.1021/acs.jpca.5b08076
J. Phys. Chem. A XXXX, XXX, XXX−XXX

photon beam and energy analyzing the resultant photodetached electrons. The photodetachment process is governed by the energy conserving relationship, $h\nu$ = EBE + EKE, where $h\nu$ is the photon energy, EBE is the electron binding (photodetachment transition) energy, and EKE is the electron kinetic energy. Our apparatus has been described previously.[23] Briefly, the apparatus consists of an ion source, a linear time-of-flight (TOF) mass spectrometer, a Nd:YAG (yttrium aluminum garnet) photodetachment laser, and a magnetic bottle photoelectron spectrometer (MB-PES). The instrumental resolution of the MB-PES is 35 meV at 1 eV EKE. The third harmonic (355 nm, 3.493 eV) of a Nd:YAG was used to photodetach the cluster anions of interest. Photoelectron spectra were calibrated against the well-known atomic transitions of Cu^-.[24]

Lanthanum cluster anions were generated in a pulsed arc cluster ionization source (PACIS) that has been described in detail previously.[25] Briefly, a discharge is triggered between an anode and a cathode that vaporizes sample from the cathode. A lanthanum rod (ESPI metals) was used as the cathode. About 150 psi of ultra-high-purity grade helium gas propelled the resultant plasma into a 10 cm flow tube, where the mixture cooled and formed cluster anions. The resulting cluster anions were monitored by the time-of-flight mass spectrometry (TOF-MS). The species of interest were then mass-selected prior to photodetachment.

III. THEORETICAL METHODS

First, we investigated the atomic species (La/La^-) in order to compare our theoretically determined EA with the previously measured[26] and our recently measured EA values. Our aim was to validate the computational approach used for the triatomic clusters. Since we are dealing with heavy atoms with incomplete 5d shell, one can expect non-negligible importance of nondynamical as well as dynamical electron correlation, especially for our ultimate goal—the La trimers. We used the state-averaged Complete Active Space (CASSCF) method[27,28] combined with the multistate second-order multiconfigurational perturbation theory (CASPT2)[29] for the dynamical correlation energy correction. Scalar relativistic effects were included via the Douglas−Kroll−Hess (DKH) approximation.[30,31] In the CASSCF step, we included 3(La)/4(La^-) active electrons distributed into 5s/5p/5d/6s/6p shells. Spin−orbit (SO) effects were added as a posteriori correction using an effective one-electron spin−orbit Hamiltonian approach.[32,33] In this treatment the SO effects are included by mixing different CASSCF wave functions under the influence of a SO Hamiltonian. The lowest 15 singlet and 15 triplet CI roots from the state-averaged CASSCF calculations were included in RASSI step. Following the strategy adopted in ref 34 the corresponding CASPT2 energies were used as diagonal elements of the SO Hamiltonian. Large contraction [11s10p8d5f3g2h] of all-electron relativistic ANO-RCC basis set[35] was used in atomic calculations. This basis set is denoted as ANO-RCC-L. We did not use relativistic pseudopotentials (e.g., cc-pVXZ-PP basis sets) because the above-mentioned a posteriori spin−orbit correction was successfully used in conjunction with the all-electron basis sets of ANO-RCC family[34,36−38] and we also wanted to avoid any possible basis set limitations in our atomic calculations. CASSCF/CASPT2 calculations were performed with the MOLCAS-6 system of programs.[39]

Computationally, neutral and anionic three-atomic lanthanum clusters are rather demanding with a large number of valence electrons and complicated electronic structure. Therefore, one must take nondynamical and dynamical electron correlations and relativistic effects into consideration in a balanced way. For the geometries, these being less sensitive to the choice of the method, we performed a systematic search for the global minimum structures using the Coalescence Kick (CK) program.[40] We adopted the Density Functional Theory (DFT) approach using the Perdew−Burke−Ernzerhof (PBE1PBE) functional and Lanl2DZ (effective core potential) basis set[41−43] for the CK search with the Gaussian09[44] program and unrestricted DFT method. Doublet, quartet, and sextet isomers were examined for the neutral species, while singlet, triplet, and quintet isomers were for the anions. Subsequently, we reoptimized the lowest structures at PBE1PBE with all-electron scalar relativistic basis set[45] and restricted RODFT method. The harmonic frequency analysis revealed that all the isomers determined in this way are minima on the potential energy surface.

Chemical bonding analysis of the La_3^- cluster was performed using double-ζ plus polarization Gaussian basis set (DZP) at the PBE1PBE/DZP[46,47] level of theory using the Adaptive Natural Density Partitioning (AdNDP) method,[48] which has been used successfully to analyze the chemical bonding of porphyrins,[49] silabenzenes,[50] mixed carbon−phosphorus,[51] carbon−boron clusters,[52] and hypervalent iodine compounds.[53] The AdNDP method[48] is an extension of the natural bonding orbital (NBO) method developed by Foster and Weinhold[54,55] and it analyzes the first-order reduced density matrix in order to obtain its local block eigenfunctions with optimal convergence properties for an electron density description. The obtained local blocks correspond to the sets of n atoms (n ranging from one to the total number of atoms in the molecule) that are tested for the presence of two-electron objects (n-center two electron (nc-2e) bonds, including core electrons and lone pairs as a special case of n = 1) associated with this particular set of n atoms. AdNDP initially searches for core electron pairs and lone pairs (1c-2e), then 2c-2e, 3c-2e, ..., and finally nc-2e bonds. At every step the density matrix is depleted of the density corresponding to the appropriate bonding elements. AdNDP accepts only those bonding elements whose occupation numbers (ONs) exceed the specified threshold values, which are usually chosen to be close to 2.00 |e|. Thus, the AdNDP method recovers both Lewis bonding elements (1c-2e and 2c-2e objects, corresponding to the core electrons and lone pairs, and two-center two-electron bonds) and delocalized bonding elements, which are associated with the concepts of aromaticity and antiaromaticity.

For the more quantitatively demanding determination of the vertical detachment energies (VDE) in La_3/La_3^-, we have chosen the following strategy. Since both La_3 and La_3^- may possess multireference character, we used the DKH-CASSCF/CASPT2 method with the relativistic ANO-RCC basis set[35] contracted to [8s7p5d3f2g1h]. This is a basis set of valence triple-ζ quality (ANO-RCC-VTZP). In the CASPT2 step, we prefer the Multi-State (MS) CASPT2 variant of the method,[29] since one can expect strong interaction between different CASSCF wave functions arising from the state averaged CASSCF. We note that the expected accuracy of CASSCF/CASPT2 with the basis set of triple-ζ quality is within 0.1−0.2 eV.[56]

From the CK search (see section IV-B-1.), it turned out that the geometries of the lowest structures are either equilateral triangle (for La_3^-) or nearly equilateral triangle (for La_3).

DOI: 10.1021/acs.jpca.5b08076
J. Phys. Chem. A XXXX, XXX, XXX−XXX

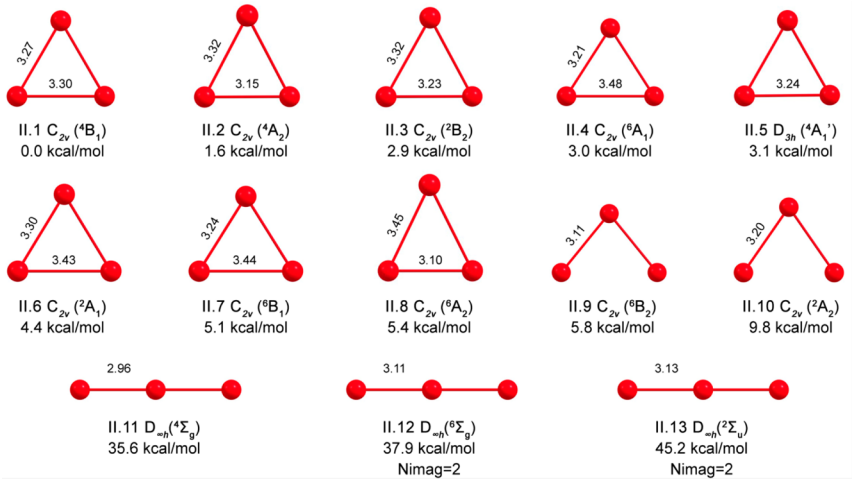

Figure 1. DFT geometries of neutral triatomic La_3 clusters. Bond lengths are given in Å.

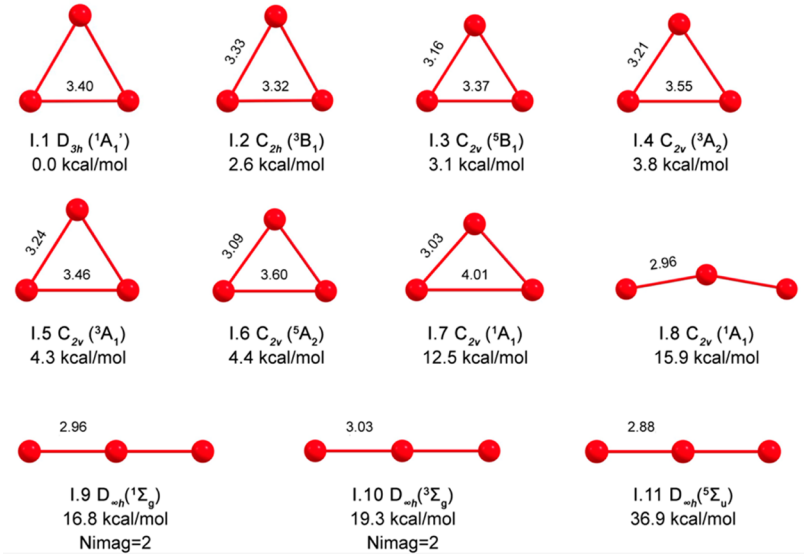

Figure 2. DFT geometries of anionic triatomic clusters, La_3^-. Bond lengths are given in Å.

Therefore, for the more demanding subsequent DKH-CASSCF/CASPT2 calculations of VDE values, we adopted a simplified computational model with an equilateral triangle and investigated potential energy curves allowing limited stretching of the La−La distance in La_3/La_3^- system. Zhang and Chen[8] have found that the difference in binding energy between equilateral and isosceles forms of neutral La_3 is only 0.01 eV which is well below the accuracy of the corresponding CASPT2 energies. In analogy to CK, a search performed at the DFT level, these potential energy curves were examined for doublet, quartet, and sextet isomers for the neutral species, and for singlet, triplet, and quintet isomers for the anions. For each multiplicity we carried out the state-averaged calculations comprising several states with equal weights that usually spanned ∼1 eV interval which was our target interval dictated by the experimental photoelectron spectrum (vide infra). In this manner one can obtain a well-balanced description of the most important states that can participate in the electron detachment process. This resulted in 8 doublet, 9 quartet, and 8 sextet states for La_3, and 9 singlet, 10 triplet, and 9 quintet states for La_3^-. When trying to average more states it turned out that there was significant gap between the lower-lying manifold and the group of higher-lying states for each multiplicity. Among the states considered in our model, one can easily identify two groups of states. The first is symmetric with respect to the symmetry plane (A′ representation or quasi Σ or Δ), and the second is antisymmetric (A″ representation or quasi Π). Although the equilateral triangular model implies the D_{3h} symmetry, and the highest Abelian group available in MOLCAS is the C_{2v}, we decided to perform all computations in C_1 symmetry. This is because when using C_{2v} symmetry in MOLCAS, the degenerate states E′ and E″ arising originally from D_{3h} group are not properly averaged since they would fall to different representations in C_{2v} (A_1 or A_2). Then, the simplest solution is the reduction of the symmetry to C_1 where *all* the states of given multiplicity are included within SA-CASSCF and, moreover, they can interact in subsequent MS-CAPT2 and RASSI procedures. So, in contrast to DFT calculations (Figures 1 and 2) we will use simplified notation of the states when discussing CASSCF/CASPT2 data.

In general, the optimal choice of the active space leads to 9 electrons/18 orbitals for La_3 and 10 electrons/18 orbitals for La_3^-. This full valence space originates from the condition that atomic 5d and 6s orbitals must constitute the final valence

DOI: 10.1021/acs.jpca.5b08076
J. Phys. Chem. A XXXX, XXX, XXX−XXX

orbitals used in CAS of the trimer. Full-valence condition can result in more than 10^7 configuration-state functions (CSFs). This is beyond the current limit for CASSCF implementation and leads to prohibitive length of computations. In such a case, one has to resort to a different strategy. Therefore, after performing several trial CASSCF runs with active orbitals ranging from 12 to 16, we applied the following criteria in the final choice of the active space: (i) select MOs with the occupation numbers ranging from 0.03 to 1.98 (for all averaged states)—very low occupation numbers (below 0.03) indicate negligible importance on the pertinent MO for all states considered in the averaging procedure; large occupation numbers (above 1.98) indicate that these orbitals are not excited in important configurations and can be omitted; (ii) select balanced number of MOs with σ-like and π-like symmetry—this criterion is important for planar systems where one expects σ- and π-aromaticity; (iii) check the shape of boundary MOs not selected on the basis of rules (i) and (ii) and add them if necessary—in general, these boundary orbitals can become more important during dissociation and their omission can lead to the occurrence of intruder states.[57] Since we scanned the potential energy curves also for stretched bonds we applied this rule in order to avoid this situation.

Criterion (i) is based on the suggestion of Gagliardi and Roos[58] and was tested in our previous work on alkali metal borides.[59] Using these criteria we arrived at 14 MOs in the active space, while keeping number of active electrons 9 for neutral and 10 for anion. The resulting number of CSFs ranged from 10^5 to 10^6. We did not consider the 4f shell because for La it is not populated. These final 14 active orbitals in the triangular geometry represent different mixing of 5d, 6s, and 6p atomic orbitals. We are aware of the limitations of the present approach; on the other hand, for the interpretation of the present experiments the accuracy of 0.1 eV seems to be satisfactory.

In MS-CASPT2[29] step we treated several states simultaneously, because this is a necessity when there are averaged states close in energy. To remove the possible intruder state problems, we used a small imaginary shift (0.05) in the energy denominators. To account for the core-correlation effects, the semicore 5s and 5p electrons also were correlated at MS-CASPT2 step. In the RASSI step—the spin−orbit part for La_3/La_3^- species—we adopted the same computational protocol as in atomic/ionic calculations. Note that the ANO-RCC basis was designed to enable inclusion of this part of core-correlation. In all trimer calculations, the ANO-RCC basis set contracted to [8s7p5d3f2g1h] was used, a relativistic all-electron basis set of valence triple-ζ quality.

IV. RESULTS AND DISCUSSION

Estimated EA and VDE values extracted from experiment are in Table 1. Comparisons of our theoretical EAs for the atom (spin-free as well as spin−orbit corrected) with the literature data are in Tables 2 and 3. The electronic selection rule states that the spin quantum number must change by 1/2; therefore, there are three possible modes of vertical electron detachment from the low lying states of La_3^- to neutral species considered in this study: (i) singlet to doublet, (ii) triplet to doublet or quartet, (iii) quintet to quartet or sextet. Tables S1−S8 (Supporting Information) comprise information on spin-free states (ordered according to occupation numbers) with different multiplicities at La−La distances referring to the energy minima of parent anions needed for the analysis of electron detachments. They contain the coefficients of the leading configurations for neutral/anionic species, their spin couplings and average occupation numbers for the most populated molecular orbitals. MO labels are only approximate, they indicate which AO-types dominantly contribute to the resulting MOs. In Tables S1 and S2 we present the leading configurations together with MO icons, spin couplings, and occupation numbers for singlet and doublet spin-free states of La_3 at R(La−La) = 3.35 Å (equilibrium distance for the lowest singlet La_3^-). In Tables S3−S5 we present the leading configurations with MO icons, spin couplings, and occupation numbers for the triplet (La_3^-), doublet and quartet spin-free states (La_3) at R(La−La) = 3.20 Å (equilibrium distance for the lowest triplet La_3^-). Finally, in Tables S6−S8 we present the leading configurations with MO icons, spin couplings, and occupation numbers for the quintet (La_3^-), quartet and sextet spin-free states (La_3) at R(La−La) = 3.00 Å (equilibrium

Table 1. Estimated EA Values of $La_{1\text{-}2,4\text{-}7}$ and VDE Values of $La_{1\text{-}2,4\text{-}7}^-$ Extracted from Experiment[a]

Species	EA	VDE
La^-	0.49	-
La_3^-	0.8	1.00
La_4^-	1.0	1.28
La_5^-	1.3	1.42
La_6^-	1.4	1.55
La_7^-	1.5	1.71

[a]All values are in eV.

Table 2. Comparison of Experimental and CASPT2/ANO-RCC-L Data for Electron Affinity of La [eV]

species	energy [Hartree]	state	EA	EA (exptl)
		spin-free data		
La	−8486.81359252	^{2}D		
La^-	−8486.82926576	^{3}F	0.426	
		spin−orbit corrected		
La^-	−8486.81644420	$^2D_{3/2}$		
La	−8486.83284087	$^3F_2$	0.446	0.47 ± 0.02, 0.5

Table 3. Comparison of Few Lowest Energy Levels [eV] for La Atom and La^-[a]

La	experiment	theory wrt $^2D_{3/2}$	La^-	theory wrt $^3F_2$
$^2D_{3/2}$	0.000	0.000	$^3D_2$	0.000
$^2D_{5/2}$	0.131	0.123	$^3F_3$	0.084
$^4F_{3/2}$	0.331	0.236	$^3G_4$	0.176
$^4F_{5/2}$	0.373	0.279	$^1D_2$	0.310
$^4F_{7/2}$	0.433	0.338	$^1D_2$	0.342
$^4F_{9/2}$	0.511	0.415	$^3D_2$	0.453
$^2F_{5/2}$	0.869	0.836	$^3S_0$	0.471
$^2F_{7/2}$	0.998	0.963	$^3P_1$	0.503
$^4P_{1/2}$	0.897	0.984	$^3F_3$	0.504
$^4P_{3/2}$	0.929	1.006	$^3P_2$	0.553
$^4P_{5/2}$	0.952	1.020	$^1G_4$	0.585
...			$^3G_5$	0.601
			$^3D_3$	0.615
			$^3F_4$	0.680

[a]Experiment taken from ref 63 Theory - CASPT2-RASSI/ANO-RCC-L data.

DOI: 10.1021/acs.jpca.5b08076
J. Phys. Chem. A XXXX, XXX, XXX−XXX

distance for the lowest quintet La_3^-). Final VDEs derived from SO analysis are collected in Table 4.

Table 4. Vertical Detachment Energies in [eV] Derived from the SO Analysis and Orbital Considerations (see also Figures 7 and 8)

parent ion		product	VDE	dominant contributing spin-free states	MO	line in Figure 8
^1A La_3^-	→	$^2A(1,2)$ $La_3 + e^-$	1.04	$0.41 \times {}^2A(1)+0.41 \times {}^2A(2)$	$3\sigma/4\sigma$	*f*
	→	$^2A(8)$ $La_3 + e^-$	1.40	$0.99 \times {}^2A(8)$	2σ	*i*
^3A La_3^-	→	$^2A(1,2)$ $La_3 + e^-$	0.70	$0.50 \times {}^2A(1)+ 0.49 \times {}^2A(2)$	2π	*b*
	→	$^2A(4)$ $La_3 + e^-$	0.77	$0.97 \times {}^2A(4)$	4σ	*c*
	→	$^2A(6)$ $La_3 + e^-$	0.85	$0.85 \times {}^2A(6)$	3σ	*e*
	→	$^4A(1,2)$ $La_3 + e^-$	0.60	$0.57 \times {}^4A(1)+ 0.38 \times {}^4A(2)$	3σ	*a*
	→	$^4A(9)$ $La_3 + e^-$	1.40	$0.99 \times {}^4A(9)$	1π	*i*
^5A La_3^-	→	$^4A(1,2)$ $La_3 + e^-$	0.79	$0.56 \times {}^4A(1)+0.44 \times {}^4A(2)$	2σ	*d*
	→	$^4A(3,4)$ $La_3 + e^-$	1.16	$0.55 \times {}^4A(3)+0.41 \times {}^4A(4)$	$1\pi/2\pi$	*h*
	→	$^6A(1)$ $La_3 + e^-$	1.06	$0.99 \times {}^6A(1)$	3δ	*g*
	→	$^6A(2)$ $La_3 + e^-$	1.16	$0.92 \times {}^6A(2)$	$1\delta/3\delta$	*h*
	→	$^6A(6)$ $La_3 + e^-$	1.49	$0.99 \times {}^6A(6)$	2δ	*j*
	→	$^6A(7)$ $La_3 + e^-$	1.62	$0.71 \times {}^6A(7)$	1δ	*k*

Figure 3 exhibits the anion photoelectron spectrum of La^- along with the photoelectron spectra of La_n^-, n = 3−7. In our experiments La_2^- was not observed. That very likely means that it was not stable. One reason could be a low or even nonpositive electron affinity of La_2. Indeed, our preliminary calculations indicated that EA for lanthanum dimer might be between 0.2 and 0.6 eV, depending on the level of theory. Recently, two papers on lanthanum dimers appeared[60,61] but none of them reported EA of La_2. Although this issue seems to be very interesting, it was not a primary focus of this paper and will be a topic of a separate project.

Experimentally determined EA values for $La_{1,3-7}$ and VDE values for $La_{1,3-7}^-$ are presented in Table 1. Given the complexity of these systems, our calculations have focused only on La^- and on La_3^-. Figures 1 and 2 contain DFT geometries and relative energies of the lowest neutral and anionic clusters. The relative energies indicate that for the subsequent CASSCF/CASPT2 calculations no linear isomers need to be considered. In Figure 4 we present AdNDP analysis of La_3^- cluster (top), electron densities of singlet La_3^- (middle) and of doublet, quartet, sextet La_3 (bottom). The division into σ- and π-density is rather pragmatic; it just reflects whether the contributing orbitals are symmetric (σ, δ) or antisymmetric (π, δ) with respect to the molecular plane. Contour levels were 0.013 for σ-densities and 0.010 for π-densities, respectively. Finally, Figures 5 and 6 show the manifolds of the limited scan−potential energy curves in the vicinity of energy minima for both spin-free model of La_3/La_3^- (Figure 5) as well as for the spin−orbit corrected model (Figure 6). In Figure 5 the lower manifold of states belongs to anions and is well separated from the upper block belonging to neutrals. In Figures 5 and 6 the energies (in eV) are relative to the lowest anionic singlet species. In Figure 7 we present a reduced picture of the detachment process at orbital level, namely, only those potential energy curves that obey the selection rule and are acceptable also according to the matching orbitals between parent anion and pertinent neutral. Finally, in Figure 8 we present the detail of the La_3^- spectrum with tentative assignments of the theoretical spin−orbit corrected VDEs (vertical lines) utilizing data from Table 4 and Figure 7.

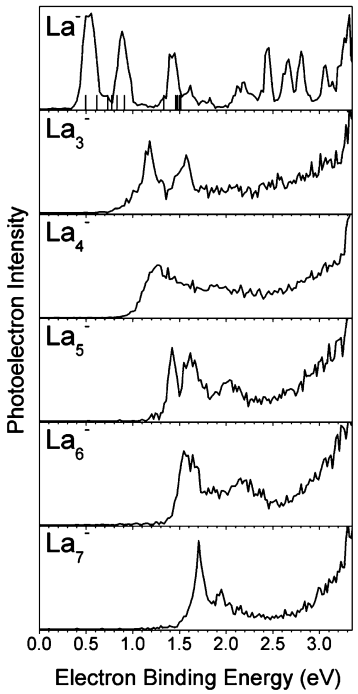

Figure 3. Anion photoelectron spectra of La^- and La_n^-, n = 3−7, measured with 355 nm photons.

A. La/La⁻ Pair. Total CASPT2/ANO-RCC-L energies for La/La^-, along with EA values, are collected in Table 2. For the EA value, we have obtained very good agreement with the current experiment (0.49 eV). The calculated results in Table 2 added by 0.49 eV (EA) are plotted as stick spectrum and embedded in the spectrum of La^- shown in Figure 3. Each of the calculated transitions is under a certain PES peak, indicating that this transition is indeed observed by experiment. Due to the resolution limit, some transitions fall within the same peak shown in the experiment. The spin-free EA value lies quite close to the experimental datum and the spin−orbit correction improves the agreement by 0.02 eV, leading to the error in EA, compared to the most recent published experiment, which is below 0.03 eV. This agreement is acceptable and in line with the expected errors in individual SO corrections predicted beyond the fifth row atoms.[34] This gives fair credibility to our computational strategy for trimers, outlined in the previous section, together with expected cancellation of these errors when evaluating the EA values. In Table 3, we present the comparison of the few lowest energy levels for La atom and La^-. It is interesting that Covington and co-workers have noted that at least one bound excited state of the anion could be observed in the photoelectron spectra, and that the respective binding energy with respect to neutral ground state lanthanum was measured to be 0.17 eV.[7] If we combine our CASPT2/

DOI: 10.1021/acs.jpca.5b08076
J. Phys. Chem. A XXXX, XXX, XXX−XXX

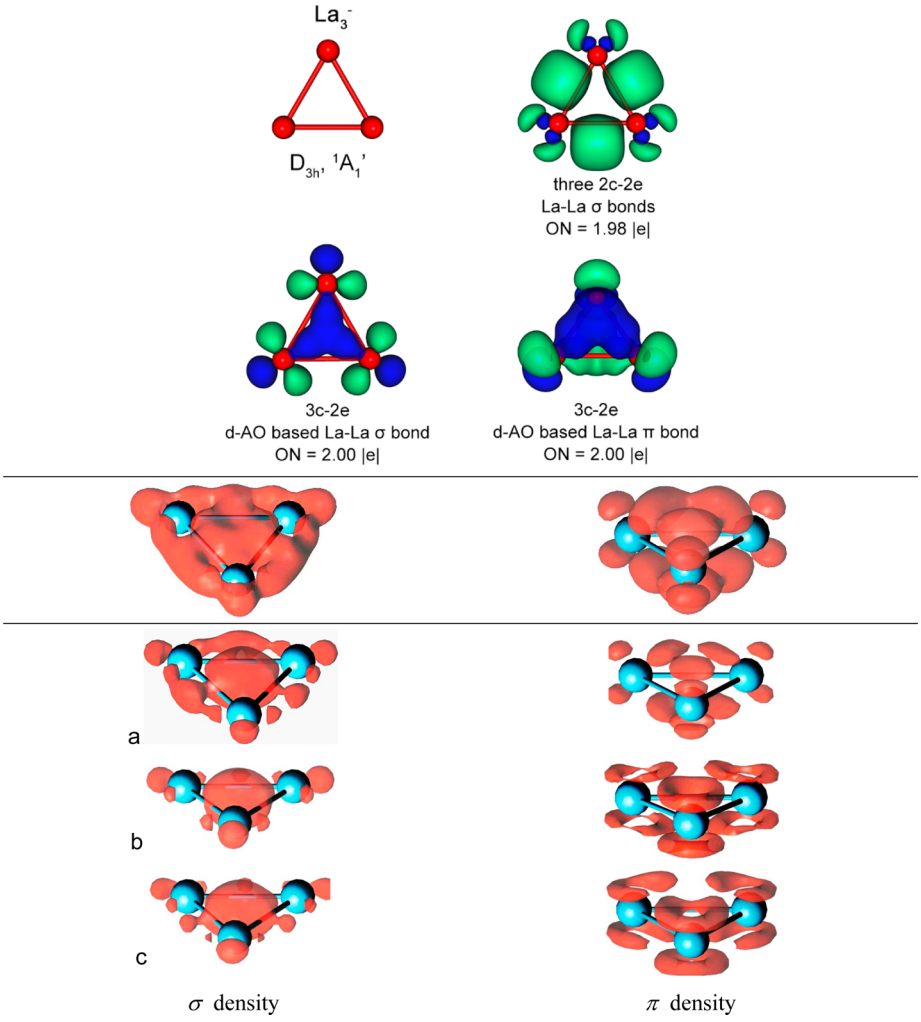

Figure 4. Top: geometric structure of La_3^-, three 2c−2e La−La σ bonds, delocalized 3c−2e d-AO based σ bond, and delocalized 3c−2e d-AO based π bond revealed by the AdNDP analysis. Middle: corresponding σ- (left) and π-electron densities (right) from CASSCF/ANO-RCC active orbitals of the lowest singlet La_3^- species. Bottom: comparison of CASSCF/ANO-RCC σ- (left) and π-electron densities (right) of neutral La_3 (a−doublet, b−quartet, c−sextet).

RASSI EA = 0.45 eV for La with this 0.17 eV, we arrive at estimated energy level 0.62 eV. Our computational approach systematically underestimates the energy levels for neutral La (Table 3, the third row) by 0.05−0.1 eV. If we expect that this error is for an anion (at least) as large as for an atom the excited state observed by Covington co-workers might correspond to above-mentioned energy level 0.62 eV and to the states between $^1G_4$ and $^3F_4$, or in the range 0.585−0.680 eV (bottom of the fourth row of Table 3). Of course, one could exploit a more elaborate, four-component relativistic approach for atomic calculations, but this would lead to a prohibitively large task in the case of La_3/La_3^- clusters.

B. Calculations of Neutral and Anionic La-Trimers. *1. DFT Geometries and Relative Energies.* The lowest energy structures of La_3^- and La_3 obtained with CK search are collected in Figures 1 and 2. In our CK procedure the triangular and/or bent structures clearly prevail among the lowest isomers, while the linear structures are either higher-order stationary points or lie too high in energy. Closer inspection of the lowest structures in the relative energy range 0−10 kcal/mol reveals that they acquire a shape of either equilateral or isosceles triangle, e.g., D_{3h} ($^1A_1'$) La_3^- is perfectly equilateral and C_{2v} ($^4B_1$) La_3 is isosceles. The deviation from equilateral triangle in the lowest La_3 isomer is fairly small, 0.03 Å. The multiplicities present in the lowest clusters (relative energy range 0−10 kcal/mol) are doublet, quartet, and sextet for neutrals and singlet, triplet, and quintet for anions. Guided by the DFT geometries and relative energies we have used these multiplicities in the CASSCF/CASPT2 calculations (sections IV-B-3 and IV-B-4) and subsequent CASPT2/RASSI runs.

2. Chemical Bonding in La_3^- Cluster. To gain more insight into the structure and chemical bonding in La_3^- cluster, we performed chemical bonding analysis of this species. The global minimum La_3^- (D_{3h}, $^1A_1'$) cluster has the following valence electronic configuration: $1a_1'^2\ 1a_2''^2\ 2a_1'^2\ 1e'^4$. The La_3^- as well as valence isoelectronic Y_3^- and Sc_3^- systems were first analyzed by Chi and Liu[62] through molecular orbital analysis. They showed that $1a_1'$ and $1e'$ molecular orbitals (MOs) are formed by the *n*s-atomic orbitals (AOs) and do not contribute to the bonding significantly, since all the bonding and antibonding MOs, which consist of the *n*s-AOs with rather small contributions from d orbitals, are occupied and the bonding effect from the $1a_1'$-MO is compensated by the antibonding effect from the $1e'$-MOs. The remaining valence MOs $1a_2''$ and $2a_1'$ are responsible for bonding in La_3^-. The $2a_1'$ MO is a bonding σ MO and renders σ aromaticity, while

DOI: 10.1021/acs.jpca.5b08076
J. Phys. Chem. A XXXX, XXX, XXX−XXX

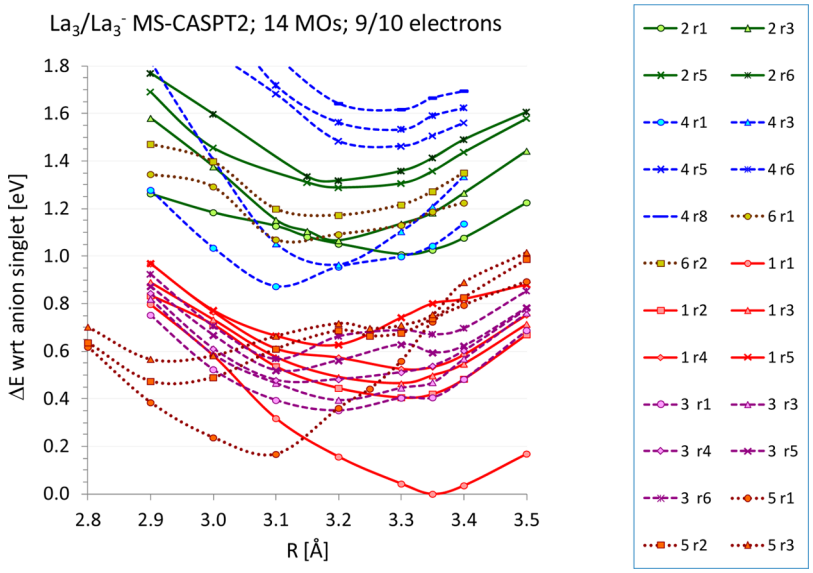

Figure 5. Spin-free MS-CASPT2 potential energy curves for La_3 and La_3^-. Multiplicities are placed to the left of the root symbol. Degenerate/quasidegenerate roots are shown only once. Solid lines—singlet/doublet species, dashed lines—triplet/quartet species, dotted lines—quintet/sextet species. We used simplified notation in legend: "*n rm*" where *n* is multiplicity and *m* is the sequence number of pertinent root.

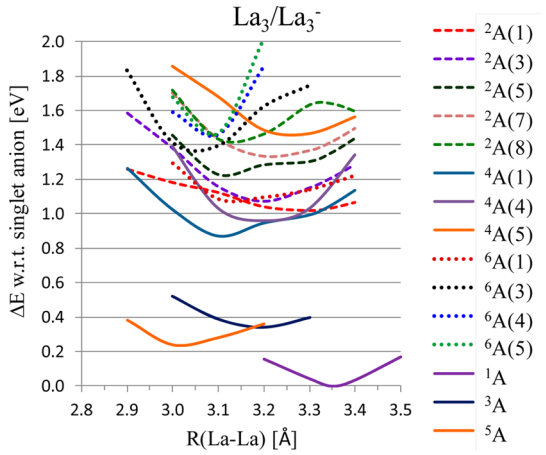

Figure 6. Spin—orbit MS-CASPT2/RASSI potential energy curves for La_3 and La_3^-. Degenerate/quasi-degenerate roots of dominant multiplicities contributing to SO states are shown only once.

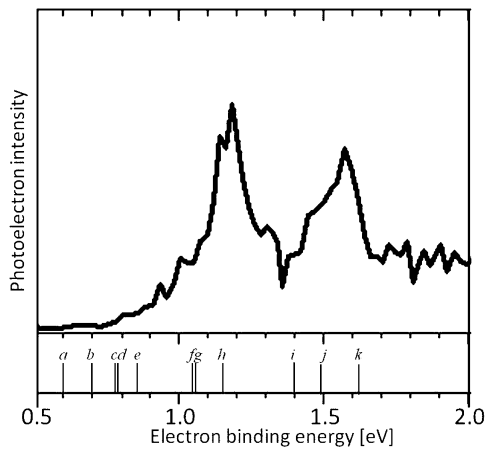

Figure 8. Detail of the anion photoelectron spectrum of La_3^- and tentative assignments of the theoretical spin—orbit corrected VDE's (vertical lines). For the legend (letters *a*—*k*) consult Table 4.

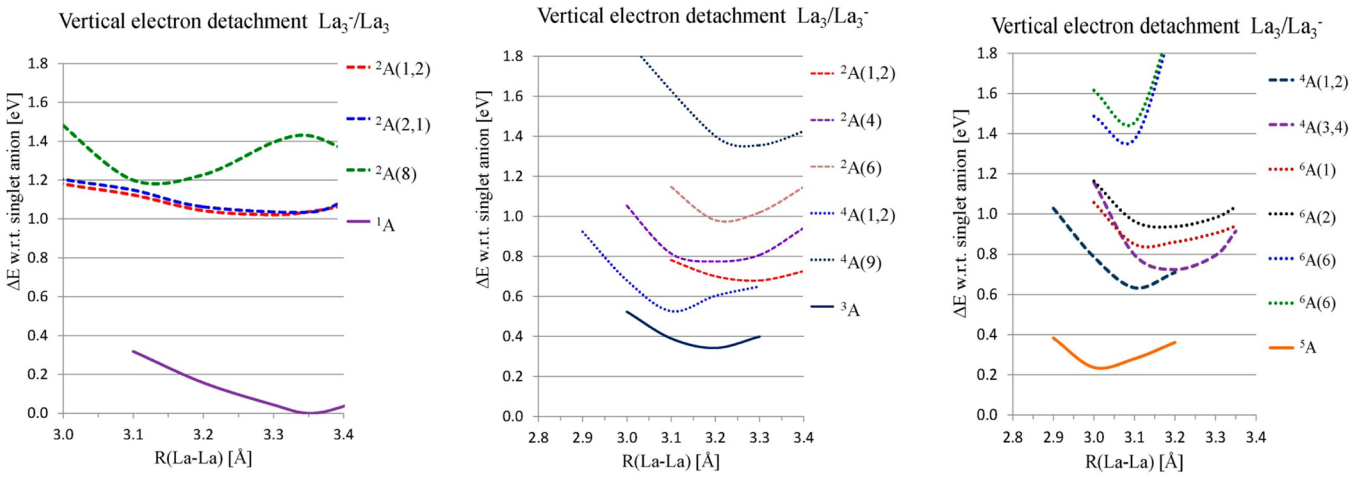

Figure 7. Illustration of the allowed detachment processes from the lowest SO-corrected singlet (left), triplet (middle), and quintet (right).

DOI: 10.1021/acs.jpca.5b08076
J. Phys. Chem. A XXXX, XXX, XXX—XXX

$1a_2''$ MO is a completely bonding π MO and is responsible for π aromaticity in La_3^- cluster. Therefore, La_3^- represents species with d-orbital based double (σ and π) aromaticity. Chi and Liu[62] also reported large negative NICS values for the La_3^-, thus supporting the presence of aromaticity in La_3^-.

The results of NBO analysis for La_3^- do not support the conclusions of Chi and Liu[62] concerning chemical bonding between La atoms. Though our NBO results at PBE1PBE/LanL2DZ are in agreement with those of the authors,[62] the calculations at higher level of theory (PBE1PBE/DZP) show that $1a_1'$ and $1e'$ MOs represent hybrids with substantial contribution from d-AOs and responsible for the formation of three 2c-2e La−La σ bonds with the following hybridization: s (48.9%), p (8.5%), d (42.6%). The results of our AdNDP analysis are consistent with the results of NBO analysis (Figure 4, top inset). The general AdNDP search revealed three 2c-2e peripheral σ bonds with occupation numbers (ON) of 1.98 |e|. In addition, the AdNDP identified one 3c-2e delocalized σ bond (ON = 2.00 |e|) and one 3c-2e π bond (ON = 2.00 |e|), highlighting double σ and π aromaticity in La_3^- cluster (Figure 4). On the basis of our AdNDP analysis we conclude that La_3^- represents an example of a d-AO doubly aromatic σ and π system, though appreciable multiconfiguratioal character of the $^1A_1'$ wave function may affect the strength of those two aromaticities.

3. Spin-Free CASSCF/CASPT2 Results for La_3 Clusters. Electron σ- and π-densities of neutral doublet, quartet, and sextet species are in the bottom inset of Figure 4 (bottom inset). Comparing these densities with the La_3^- cluster, one can see that shapes of the doublet densities qualitatively map onto the singlet ones, just reflecting the effect of the detached electron. The quartet and sextet densities reveal the gradual reduction of the σ-subspace on account of promoting unpaired electrons to the density in π-subspace. The coefficients of the leading configurations and fractional occupancies clearly indicate that all the neutral trimer species possess significant multireference character, so the choice of state-averaged strategy in CASSCF/CASPT2 steps is justified. In terms of energy (Figure 5), the neutral trimers lie quite close to each other at crucial distances (3.00, 3.20, and 3.35 A), they can easily interact, and so for the subsequent comparison with the experimental spectrum, all three multiplicities might be important.

The manifold of CASPT2 potential energy curves are in Figure 5, for better visibility degenerate/quasi-degenerate roots are shown only once and the energies are relative to the lowest La_3^- singlet species. The lowest La_3 structure found with the 3.0−3.4 Å interval is the quartet, in agreement with the DFT $^4B_1$ structure (Figure 1) but the CASPT2 equilibrium distance is shorter (R(La−La) = 3.116 Å). The lowest doublet La_3 has optimum R(La−La) = 3.289 Å, which is in good agreement with the DFT $^2B_2$ structure (Figure 1). The lowest sextet state acquires CASPT2 equilibrium distance R(La−La) = 3.141 Å. Tentatively, we can match the computed spin-free CASPT2 states with the features in Figure 3 for this La−La distance. The ordering of the first three states from CASPT2 calculations follows the ordering obtained from DFT ones and their energies (relative to La_3^- singlet) correspond with the observed small features of the final neutral state in the photoelectron spectrum between 0.9 and 1.1 eV. The rest of the curves in the manifold in Figure 5 are rather dense and their energies can be attributed to peaks between 1.2 and 2.0 eV in the photoelectron spectrum. We postpone more detailed bottom-line discussion and comparisons on electron detachments to the spin−orbit section.

4. Spin-Free CASSCF/CASPT2 Results for La_3^- Clusters. The shapes of active MOs selected for La_3^- singlets, triplets, and quintets used in DKH-CASSCF/CASPT2 calculations are displayed in Tables S1, S3, and S6 (see Supporting Information). In the lowest La_3^- singlet, with equilibrium distance R(La−La) = 3.35 Å, the closed-shell configuration is dominating, so one can expect only second-order spin−orbit contribution for this closed-shell anion. This closed-shell domination can be clearly seen also in the middle part of Figure 4 where the CASSCF σ- and π-electron densities for the lowest singlet species nicely match the 2c-2e and 3c-2e σ-bonds as well as the 3c-2e π-bond revealed by AdNDP analysis from DFT calculation (top inset of Figure 4). In the lowest La_3^- triplet the equilibrium distance is shorter; R(La−La) = 3.20 Å, while the lowest quintet has the shortest R(La−La) = 3.00 Å. One can expect that the dominant contribution coming from the vertical electron detachment process to the peaks observed in the La_3^- spectrum will arise from these lowest singlet, triplet, and quintet states at their pertinent equilibrium distances (Tables S1, S3, and S6 in Supporting Information) that span a relatively small energy gap 8 kcal/mol and are distinctively separated from the rest of the manifold in Figures 5 and 6. Keeping in mind the spin selection rule, we shall analyze the spin orbit results combining the possible vertical electron detachments as follows: (i) R(La−La) = 3.35 Å, detachment from the lowest singlet La_3^- to doublet La_3; (ii) R(La−La) = 3.20 Å, detachment from the lowest triplet La_3^- to doublet/quartet La_3; (iii) R(La−La) = 3.00 Å, detachment from lowest quintet La_3^- to quartet/sextet La_3.

5. Spin−Orbit CASPT2/RASSI Results. The manifold of potential energy curves resulting from spin−orbit MS-CASPT2/RASSI calculations are displayed in Figure 6. The analysis of the weights of the five most important spin-free states for both the neutral and anionic species revealed that the majority of the low-lying spin−orbit states are dominated by the original spin-free ones with the weights ranging from 0.99 to 0.70; thus, the state interaction is only small-to-moderate. There are a few exceptions in this picture: spin−orbit states composed of doublets are usually a mixture of two lowest spin-free doublet states, and the same holds for quartets (cf. Table 4). For this situation we use the notation, e.g., $^2A(1,2)$, reflecting that two doublet spin-free roots 1 and 2 contribute to the mixed SO-state. For the majority of other cases one can conclude that the CASPT2/RASSI correction represents the second-order SO effect.

Figure 6 reveals that the spin−orbit corrections only moderately affect both the manifold of neutral states (especially between 3.0 and 3.2 Å), leading to numerous avoided crossings. The most significant change upon SO-coupling is the change in equilibrium La−La distance for the lowest quintet anionic state, which is shifted to 3.0 Å. Spin−orbit corrections in La_3^- also result in approach of the (originally) spin-free triplet and quintet curves. This is probably the result of the stronger spin−orbit interaction between the manifold of triplet and quintet states. Otherwise, the overall pattern of the spin−orbit curves does not differ significantly from the spin-free ones and indicated only slight stabilization of higher multiplicities in the La_3/La_3^- clusters. For the subsequent discussion, the lowest anionic states will serve as the energy reference.

6. Vertical Detachment Energies—Comparison with the Anion Photoelectron Spectrum. From our calculations we can

DOI: 10.1021/acs.jpca.5b08076
J. Phys. Chem. A XXXX, XXX, XXX−XXX

also deduce the vertical electron affinities (VEA). For VEA one must consider neutral as a parent system in its equilibrium geometry. Using the spin-free data in Figure 5 one can expect that the dominant contribution to VEA can come from the minima corresponding to sextet/quintet, doublet/triplet, and from doublet/singlet electron attachments. The corresponding vertical energy differences yield VEA values in the range 0.7−1.0 eV which can be accepted as a lower and upper bound of EA and are in good agreement with our experimental value 0.8 eV. With accuracy of CASPT2 method (±0.1−0.2 eV) in mind, this is still an acceptable lower bound for VEA. SO corrections are small and change shifts the lower bound to 0.8 eV.

The experimental photoelectron spectrum of La_3^- (Figure 3) exhibits several distinct peaks that can be compared with MS-CASPT2/RASSI data in Figures 6 and 7. For the assignment in which we use the electronic selection rule that the spin quantum number must change by 1/2, the pertinent *possible* detachment routes are summarized in Table 4 and Figure 8. Electron detachment from the singlet state will produce the doublet, electron detachment from a triplet will produce either doublet or quartet, and electron detachment from a quintet will produce either quartet or sextet. However, adding the orbital considerations (σ/π symmetries, spin couplings, and occupation numbers) we can reduce this set to only those detachments in which one can find matching MOs.

The vertical detachment energies corrected for spin−orbit coupling can be calculated from the minima on the potential curves of anions with respect to the corresponding energy points on the potential curve of neutrals (Figure 7). The most important parent states for the detachment process are the states dominated by closed-shell singlet (R_e = 3.35 Å), by the quintet state (R_e = 3.1 Å, lying approximately 0.24 eV above) and by the triplet (R_e = 3.2 Å, ∼0.36 eV above singlet). The parent anionic states (^{1}A, ^{3}A, and ^{5}A) span the interval of energies easily accessible within the collision process during the generation of anions.

Starting from the parent states one can deduce the approximate matches with the peaks recorded in the La_3^- spectrum as summarized in Table 4. In light of the accuracy of the CASPT2/RASSI method,[34,56] especially for heavy elements, there are roughly three typical patterns of theoretical "lines": *a*−*e*, *f*−*h*, and *i*−*k* that can be compared with the peaks in La_3^- spectrum (Figure 8). The minute, low-intensity feature around 0.8−1.0 eV can be associated with the vertical transition *a*−*e*; they refer either to detachment from ^{3}A state to ^{2}A (doublet roots 1, 2, 4, and 6) or ^{4}A (quartet roots 1, 2, and 9). For example, the detachment process $^3\mathrm{A} \rightarrow {}^2\mathrm{A}(1,2)$ can be associated with emptying the orbital 2π (Tables S3 and S4, compare roots with CSF coefficient 0.632 in triplet and 0.732 in doublet). Similar matching VDEs and participating orbitals (σ/δ) can be found for the next three lines *f*−*h* in the range 1.0−1.2 eV; they fit within the computational accuracy to the first significant experimental peak around 1.1−1.2 and contributing detachments are $^1\mathrm{A} \rightarrow {}^2\mathrm{A}(1,2)$, $^5\mathrm{A} \rightarrow {}^6\mathrm{A}(1)$, and $^5\mathrm{A} \rightarrow {}^6\mathrm{A}(2)$. The last three theoretical lines *i*−*k* belong approximately to the second peak at 1.5−1.6 eV and contributing detachments are $^1\mathrm{A} \rightarrow {}^2\mathrm{A}(8)$, $^5\mathrm{A} \rightarrow {}^6\mathrm{A}(6)$, and $^5\mathrm{A} \rightarrow {}^6\mathrm{A}(7)$.

This analysis revealed that all spin-free states considered in both neutral and anionic lanthanum trimers play equally important roles in the spin−orbit mixing and, subsequently, in the interpretation of anion photoelectron spectrum of La_3^-. Detailed orbital considerations revealed that not all of the roots included in CASSCF/CASPT2 calculations are directly involved in the electron detachment process due to absence of matching molecular orbitals.

C. Conclusions. A combined experimental and theoretical investigation of small lanthanum clusters in the gas phase is reported. Electron affinities (EAs) and vertical electron detachment energies (VDEs) of La_n^- (n = 3−7) clusters were experimentally measured for the first time. Multiple peaks in the experimental photoelectron spectra and the broad shape of many peaks indicate a high density of electronic states for the La anions and corresponding neutral species. We theoretically evaluated EAs and VDEs for the La^- and La_3^- simplest species with experimental accuracy using large-scale multiconfigurational calculations including relativistic corrections. The presented level of theory reproduces an experimental electronic excitation spectrum of La within 0.1 eV and the experimental EA of La within 0.02 eV. However, even for the smallest La_3^- cluster we observed a significant multiconfigurational character of wave functions for both neutral and anionic states. Therefore, accurate La cluster calculations, which take into account the multiconfigurational nature of wave function and relativistic effects, represent a very challenging task for modern quantum chemistry. Analysis of chemical bonding in the La_3^- global minimum structure shows that this anion can be considered as an example of d-AO based double σ and π aromaticity.

■ ASSOCIATED CONTENT

Supporting Information

The Supporting Information is available free of charge on the ACS Publications website at DOI: 10.1021/acs.jpca.5b08076.

Tables S1−S8: information on spin-free states (ordered according to occupation numbers), coefficients of the leading configurations for neutral/anionic species, spin couplings, average occupation numbers for the most populated molecular orbitals, MO icons and labels indicating which AO-types dominantly contribute to the resulting MOs (PDF)

■ AUTHOR INFORMATION

Corresponding Author

*E-mail: cernusak@fns.uniba.sk.

Author Contributions

#A.S. Ivanov and X. Zhang contributed equally.

Notes

The authors declare no competing financial interest.

■ ACKNOWLEDGMENTS

A.I.B. appreciates funding from the J. W. Fulbright Commission for his work at Comenius University in Bratislava. Research performed at Comenius University was supported by Slovak Grant Agency (Grant VEGA 1/0092/14). Research performed at Utah State University (A.I.B.) was supported by the US National Science Foundation (CHE-1111693 and award CHE-1361413). We thank the Division of Research Computing in the Office of Research and Graduate Studies at Utah State University. The experimental part of this material is based upon work supported by the US National Science Foundation under Grant Number CHE-1360692 (K.H.B.). Part of the calculations were performed in the Computing Centre of the Slovak Academy of Sciences using the supercomputing infrastructure acquired in project ITMS 26230120002 and 26210120002 (Slovak infrastructure for high-performance computing)

DOI: 10.1021/acs.jpca.5b08076
J. Phys. Chem. A XXXX, XXX, XXX−XXX

supported by the Research & Development Operational Programme funded by the ERDF.

REFERENCES

(1) Kumar, R. A.; Arivanandhan, M.; Hayakawa, Y. Recent Advances in Rare Earth-Based Borate Single Crystals: Potential Materials for Nonlinear Optical and Laser Applications. *Prog. Cryst. Growth Charact. Mater.* **2013**, *59*, 113−132.

(2) Zhu, X.; Peyghambarian, N. High-Power ZBLAN Glass Fiber Lasers: Review and Prospect. *Adv. OptoElectron.* **2010**, *2010*, 501956.

(3) Zhan, W.; Guo, Y.; Gong, X.; Guo, Y.; Wang, Y.; Lu, G. Current Status and Perspectives of Rare Earth Catalytic Materials and Catalysis. *Chin. J. Catal.* **2014**, *35*, 1238−1250.

(4) Trenary, M. Surface Science Studies of Metal Hexaborides. *Sci. Technol. Adv. Mater.* **2012**, *13*, 023002.

(5) Cahay, M.; Boolchand, P.; Fairchild, S. B.; Grazulis, L.; Murray, P. T.; Back, T. C.; Semet, V.; Binh, V. T.; Wu, X. H.; Poitras, D.; et al. Review Article: Rare-Earth Monosulfides as Durable and Efficient Cold Cathodes. *J. Vac. Sci. Technol. B* **2011**, *29*, 06F602.

(6) Kim, J.; Lee, J.-H.; An, H.; Lee, J.; Park, S.-H.; Seo, Y.-S.; Miller, W. H. Luminescence Properties of LaF_3:Ce Nanoparticles Encapsulated by Oleic Acid. *Mater. Res. Bull.* **2014**, *57*, 110−115.

(7) Covington, A. M.; Calabrese, D.; Thompson, J. S.; Kvale, T. J. Measurement of the Electron Affinity of Lanthanum. *J. Phys. B: At., Mol. Opt. Phys.* **1998**, *31*, L855−L860.

(8) Zhang, D.-B.; Shen, J. Ground State, Growth, and Electronic Properties of Small Lanthanum Clusters. *J. Chem. Phys.* **2004**, *120*, 5104−5109.

(9) Lyalin, A.; Solov'yov, A. V.; Greiner, W. Structure and Magnetism of Lanthanum Clusters. *Phys. Rev. A: At., Mol., Opt. Phys.* **2006**, *74*, 043201.

(10) Meng, J. H.; Deng, X. J.; Li, Z. Y.; He, S. G.; Zheng, W. J. Thermal Methane Activation by $La_6O_{10}^-$ Cluster Anions. *Chem. - Eur. J.* **2014**, *20*, 5580−5583.

(11) Rutkowski, P. X.; Michelini, M. C.; Gibson, J. K. Gas-Phase Lanthanide Chloride Clusters: Relationships Among ESI Abundances and DFT Structures and Energetics. *Phys. Chem. Chem. Phys.* **2012**, *14*, 1965−1977.

(12) Xie, H.; Wang, J.; Qin, Z. B.; Shi, L.; Tang, Z. C.; Xing, X. P. Octacoordinate Metal Carbonyls of Lanthanum and Cerium: Experimental Observation and Theoretical Calculation. *J. Phys. Chem. A* **2014**, *118*, 9380−9385.

(13) Xu, B.; Zhao, Y. X.; Ding, X. L.; He, S. G. Reactions of $Sc_2O_4^-$ and $La_2O_4^-$ Clusters with CO: A Comparative Study. *Int. J. Mass Spectrom.* **2013**, *334*, 1−7.

(14) Xu, B.; Zhao, Y. X.; Li, X. N.; Ding, X. L.; He, S. G. Experimental and Theoretical Study of Hydrogen Atom Abstraction from n-Butane by Lanthanum Oxide Cluster Anions. *J. Phys. Chem. A* **2011**, *115*, 10245−10250.

(15) Knight, J. L. B.; Woodward, R. W.; Van Zee, R. J.; Weltner, J. W. Properties of Sc_3, Y_3, and Sc_{13} Molecules at Low Temperatures, as Determined by ESR. *J. Chem. Phys.* **1983**, *79*, 5820−5827.

(16) Finlayson-Pitts, B. J.; Pitts, J. N., Jr. *Chemistry of the Upper and Lower Atmosphere: Theory, Experiments, and Applications*; Academic Press: San Diego/London, 1999.

(17) Fantz, U.; Falter, H. D.; Franzen, P.; Speth, E.; Hemsworth, R.; Boilson, D.; Krylov, A. Plasma Diagnostic Tools for Optimizing Negative Hydrogen Ion Sources. *Rev. Sci. Instrum.* **2006**, *77*, 03A516.

(18) Hotop, H.; Lineberger, W. C. Binding Energies in Atomic Negative Ions. *J. Phys. Chem. Ref. Data* **1975**, *4*, 539−576.

(19) Hotop, H.; Lineberger, W. C. Binding-Energies in Atomic Negative-Ions. 2. *J. Phys. Chem. Ref. Data* **1985**, *14*, 731−750.

(20) Andersen, T.; Haugen, H. K.; Hotop, H. Binding Energies in Atomic Negative Ions: III. *J. Phys. Chem. Ref. Data* **1999**, *28*, 1511−1533.

(21) Snodgrass, J. T.; Coe, I. V.; Freidhoff, C. B.; McHugh, K. M.; Bowen, K. H. Negative-Ion Photoelectron-Spectroscopy of P_2. *Chem. Phys. Lett.* **1985**, *122*, 352−355.

(22) Xu, C. S.; deBeer, E.; Neumark, D. M. Photoelectron Spectroscopy of PO_2. *J. Chem. Phys.* **1996**, *104*, 2749−2751.

(23) Gerhards, M.; Thomas, O. C.; Nilles, J. M.; Zheng, W. J.; Bowen, K. H. Cobalt-Benzene Cluster Anions: Mass Spectrometry and Negative Ion Photoelectron Spectroscopy. *J. Chem. Phys.* **2002**, *116*, 10247−10252.

(24) Ho, J.; Ervin, K. M.; Lineberger, W. C. Photoelectron-Spectroscopy of Metal Cluster Anions - CuN^-, AgN^-, and AuN^-. *J. Chem. Phys.* **1990**, *93*, 6987−7002.

(25) Zhang, X. X.; Wang, Y.; Wang, H. P.; Lim, A.; Gantefoer, G.; Bowen, K. H.; Reveles, J. U.; Khanna, S. N. On the Existence of Designer Magnetic Superatoms. *J. Am. Chem. Soc.* **2013**, *135*, 4856−4861.

(26) Covington, A. M. Laser Photodetached Electron Spectroscopy of Atomic Negative Ions; Doctoral thesis; University of Nevada, 1998.

(27) Andersson, K.; Malmqvist, P.-A.; Roos, B.; Sadlej, A. J.; Wolinski, K. Second Order Multiconfigurational Perturbation Theory. *J. Phys. Chem.* **1990**, *94*, 5483−5488.

(28) Andersson, K.; Malmqvist, P.-A.; Roos, B. Second-Order Perturbation Theory with a Complete Active Space Self-Consistent Field Reference Function. *J. Chem. Phys.* **1992**, *96*, 1218−1226.

(29) Finley, J.; Malmqvist, P. A.; Roos, B. O.; Serrano-Andres, L. The Multi-State CASPT2Method. *Chem. Phys. Lett.* **1998**, *288*, 299−306.

(30) Douglas, M.; Kroll, N. M. Quantum Electrodynamical Corrections to the Fine Structure of Helium. *Ann. Phys. (Amsterdam, Neth.)* **1974**, *82*, 89−155.

(31) Hess, B. A. Relativistic Electronic-Structure Calculations Employing a 2-Component No-Pair Formalism with External-Field Projection Operators. *Phys. Rev. A: At., Mol., Opt. Phys.* **1986**, *33*, 3742−3748.

(32) Hess, B. A.; Marian, C. M.; Wahlgren, U.; Gropen, O. A Mean-Field Spin-Orbit Method Applicable to Correlated Wavefunctions. *Chem. Phys. Lett.* **1996**, *251*, 365−371.

(33) Ilias, M.; Kello, V.; Urban, M. Relativistic Effects in Atomic and Molecular Properties. *Acta Phys. Slovaca* **2010**, *60*, 259−391.

(34) Roos, B.; Malmqvist, P.-A. Relativistic Quantum Chemistry: the Multiconfigurational Approach. *Phys. Chem. Chem. Phys.* **2004**, *6*, 2919−2927.

(35) Roos, B. O.; Lindh, R.; Malmqvist, P. A.; Veryazov, V.; Widmark, P. O. New Relativistic ANO Basis Sets for Transition Metal Atoms. *J. Phys. Chem. A* **2005**, *109*, 6575−6579.

(36) Demovic, L.; Cernusak, I.; Theodorakopoulos, G.; Petsalakis, I. D.; Urban, M. Improved Theoretical Calculations of InN in Its X^3S^- Ground State and in the First ^3P Excited State. *Chem. Phys. Lett.* **2007**, *447*, 215−220.

(37) Iliaš, M.; Aa. Jensen, H. J.; Kellö, V.; Roos, B. O.; Urban, M. Theoretical Study of PbO and the PbO Anion. *Chem. Phys. Lett.* **2005**, *408*, 210−215.

(38) Roos, B. O.; Malmqvist, P.-Å. On the Effects of Spin−Orbit Coupling on Molecular Properties: Dipole Moment and Polarizability of PbO and Spectroscopic Constants for the Ground and Excited States. *Adv. Quantum Chem.* **2004**, *47*, 37−49.

(39) Aquilante, F.; De Vico, L.; Ferre, H.; Ghigo, G.; Malmqvist, P. A.; Neograd y, P.; Pedersen, T.; Pitonak, M.; Reiher, M.; Roos, B.; et al. MOLCAS 7: The Next Generation. *J. Comput. Chem.* **2010**, *31*, 224−247.

(40) Sergeeva, A. P.; Averkiev, B. B.; Zhai, H. J.; Boldyrev, A. I.; Wang, L. S. All-Boron Analogues of Aromatic Hydrocarbons: B_{17}^- and B_{18}^-. *J. Chem. Phys.* **2011**, *134*, 224304.

(41) Hay, P. J.; Wadt, W. R. Ab Initio Effective Core Potentials for Molecular Calculations - Potentials for the Transition-Metal Atoms Sc to Hg. *J. Chem. Phys.* **1985**, *82*, 270−283.

(42) Wadt, W. R.; Hay, P. J. Ab Initio Effective Core Potentials for Molecular Calculations - Potentials for Main Group Elements Na to Bi. *J. Chem. Phys.* **1985**, *82*, 284−298.

(43) Hay, P. J.; Wadt, W. R. Ab Initio Effective Core Potentials for Molecular Calculations - Potentials for K to Au Including the Outermost Core Orbitals. *J. Chem. Phys.* **1985**, *82*, 299−310.

DOI: 10.1021/acs.jpca.5b08076
J. Phys. Chem. A XXXX, XXX, XXX−XXX

(44) Frisch, M. J.; Trucks, G. W.; Schlegel, H. B.; Scuseria, G. E.; Robb, M. A.; Cheeseman, J. R.; Scalmani, G.; Barone, V.; Mennucci, B.; Petersson, G. A.; et al.; *Gaussian 09*, Revision A.02; Gaussian, Inc., Wallingford CT, 2009.
(45) Pantazis, D. A.; Neese, F. All-Electron Scalar Relativistic Basis Sets for the Lanthanides. *J. Chem. Theory Comput.* **2009**, *5*, 2229−2238.
(46) Dunning, T. H. Gaussian Basis Functions for Use in Molecular Calculations. III. Contraction of (10s6p) Atomic Basis Sets for the First-Row Atoms. *J. Chem. Phys.* **1971**, *55*, 716−723.
(47) McLean, A. D.; Chandler, G. S. Contracted Gaussian Basis Sets for Molecular Calculations. I. Second Row Atoms, Z = 11−18. *J. Chem. Phys.* **1980**, *72*, 5639−5648.
(48) Zubarev, D. Y.; Boldyrev, A. I. Developing Paradigms of Chemical Bonding: Adaptive Natural Density Partitioning. *Phys. Chem. Chem. Phys.* **2008**, *10*, 5207−5217.
(49) Ivanov, A. S.; Boldyrev, A. I. Deciphering Aromaticity in Porphyrinoids via Adaptive Natural Density Partitioning. *Org. Biomol. Chem.* **2014**, *12*, 6145−6150.
(50) Ivanov, A. S.; Boldyrev, A. I. $Si_{6-n}C_nH_6$ (n = 0−6) Series: When Do Silabenzenes Become Planar and Global Minima? *J. Phys. Chem. A* **2012**, *116*, 9591−9598.
(51) Ivanov, A. S.; Bozhenko, K. V.; Boldyrev, A. I. Peculiar Transformations in the $C_xH_xP_{4-x}$ (x = 0−4) Series. *J. Chem. Theory Comput.* **2012**, *8*, 135−140.
(52) Galeev, T. R.; Ivanov, A. S.; Romanescu, C.; Li, W.-L.; Bozhenko, K. V.; Wang, L.-S.; Boldyrev, A. I. Molecular Wheel to Monocyclic Ring Transition in Boron-Carbon Mixed Clusters $C_2B_6^-$ and $C_3B_5^-$. *Phys. Chem. Chem. Phys.* **2011**, *13*, 8805−8810.
(53) Ivanov, A. S.; Popov, I. A.; Boldyrev, A. I.; Zhdankin, V. V. The I = X (X═O,N,C) Double Bond in Hypervalent Iodine Compounds: Is it Real? *Angew. Chem., Int. Ed.* **2014**, *53*, 9617−9621.
(54) Foster, J. P.; Weinhold, F. Natural Hybrid Orbitals. *J. Am. Chem. Soc.* **1980**, *102*, 7211−7218.
(55) Weinhold, F.; Landis, C. R. *Valency and Bonding, A Natural Bond Orbital Donor−Acceptor Perspective*; Cambridge University Press: Cambridge, 2005.
(56) Azizi, Z.; Roos, B. O.; Veryazov, V. How Accurate is the CASPT2Method? *Phys. Chem. Chem. Phys.* **2006**, *8*, 2727−2732.
(57) Forsberg, N.; Malmqvist, P.-Å. Multiconfiguration Perturbation Theory with Imaginary Level Shift. *Chem. Phys. Lett.* **1997**, *274*, 196−204.
(58) Gagliardi, L.; Roos, B. O. Multiconfigurational Quantum Chemical Methods for Molecular Systems Containing Actinides. *Chem. Soc. Rev.* **2007**, *36*, 893−903.
(59) Cukovicova, M.; Federic, J.; Cernusak, I. Alkali Metal Borides MeB (Me = Li, Na, K, Rb, Cs, Fr): CASPT2 Calculations. *Int. J. Quantum Chem.* **2011**, *111*, 3438−3451.
(60) Liu, Y.; Fang, L.; Shen, X.; Chen, X.; Lombardi, J. R.; Lindsay, D. M. Absorption, Resonance Raman and Raman Excitation Spectra of Lanthanum Dimers in Argon Matrices. *Chem. Phys.* **2000**, *262*, 25−29.
(61) Cao, X. Y.; Dolg, M. Pseudopotential Study of Lanthanum and Lutetium Dimers. *Theor. Chem. Acc.* **2002**, *108*, 143−149.
(62) Chi, X. X.; Liu, Y. Theoretical Evidence of d-Orbital Aromaticity in Anionic Metal X_3^- (X = Sc, Y, La) Clusters. *Int. J. Quantum Chem.* **2007**, *107*, 1886−1896.
(63) Martin, W. C.; Zalubas, R.; Hagan, L. Atomic Energy Levels - the Rare-Earth Elements; *Natlional Standards Reference Data Series*; National Bureau of Standards: Washington, DC, 1978; Vol. *60*.

DOI: 10.1021/acs.jpca.5b08076
J. Phys. Chem. A XXXX, XXX, XXX−XXX